FLOW PATTERNS NEAR CODIMENSION-2 BIFURCATION IN NON-BOUSSINESQ MIXED CONVECTION

Sergey A. Suslov

Department of Mathematics and Computing, University of Southern Queensland, Toowoomba, Queensland 4350, Australia
E-mail: ssuslov@usq.edu.au

Abstract

Realistic nonlinear (non-Boussinesq) fluid property variations with temperature (expressed, for example, by the Sutherland formulae for viscosity and thermal conductivity and by the ideal gas equation of state for the density) are shown to lead to a rich variety of flow instability phenomena in the classical problem of mixed convection in a differentially heated vertical channel. The instabilities are caused by competing buoyancy and shear effects. One of the most complicated and interesting flow regimes arises when two instability modes bifurcate simultaneously at the so-called codimension-2 point. It is shown that such a situation can be modelled successfully by coupled cubic complex Landau-type equations derived using a weakly nonlinear stability theory. In this paper the unfoldings of one of the double Hopf bifurcations detected in non-Boussinesq mixed convection are investigated. The complete set of resulting flow patterns is studied as functions of governing physical parameters. This paper complements a general classification of unfoldings of codimension-2 bifurcations and interprets the results obtained for the model dynamical system from the physical point of view.

Introduction and problem definition

Consider a flow of air with the average (reference) temperature $T_r = 300K$ whose density ρ, dynamic viscosity μ, thermal conductivity k and specific heat c_p nondimensionalised with respect to their values at T_r vary with temperature T according to the ideal gas and Sutherland formulae

$$\rho T = 1, \quad \mu = T^{3/2}\frac{1.368}{T+0.368}, \quad k = T^{3/2}\frac{1.648}{T+0.648}, \quad c_p = 1 \tag{1}$$

between two isothermal vertical plates separated by the gap of width H and maintained at different temperatures T_h and T_c, $T_h > T_c$. As discussed in [1] such flow is described by the Low-Mach-Number equations

$$\frac{\partial \rho}{\partial t} + \frac{\partial \rho u_i}{\partial x_i} = 0\,, \tag{2}$$

$$\frac{\partial \rho u_i}{\partial t} + \frac{\partial \rho u_i u_j}{\partial x_j} = -\frac{\partial \Pi}{\partial x_i} + \frac{Gr}{2\epsilon}(\rho - 1)n_i + \frac{\partial \tau_{ij}}{\partial x_j} \tag{3}$$

$$\rho c_p \left(\frac{\partial T}{\partial t} + u_j \frac{\partial T}{\partial x_j}\right) = \frac{1}{Pr}\frac{\partial}{\partial x_j}\left(k\frac{\partial T}{\partial x_j}\right)\,, \tag{4}$$

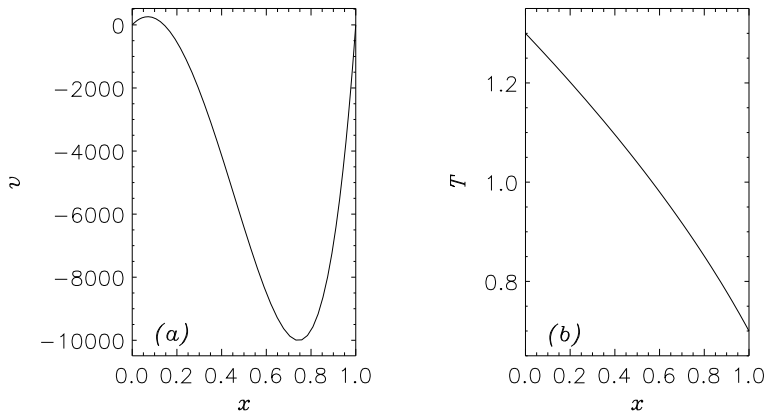

Figure 1: Basic flow velocity (a) and temperature (b) profiles at the codimension-2 point $(Gr_*, Re_*) = (526921.8, -5179.405)$.

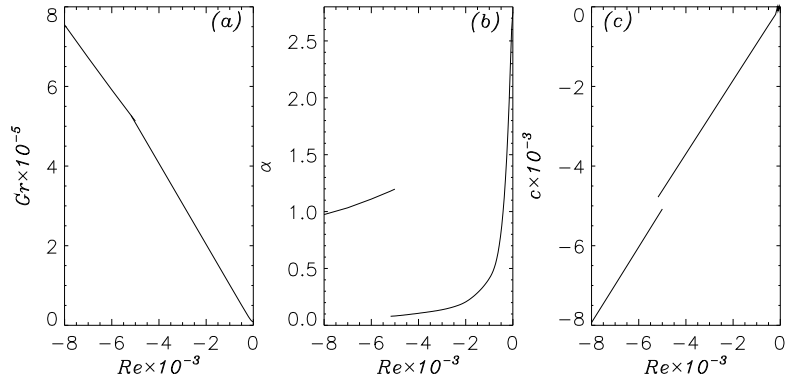

Figure 2: Linear stability diagram for mixed convection in a vertical channel for $\epsilon = 0.3$.

where the Grashof, Reynolds and Prandtl numbers and non-dimensional temperature difference between the walls are defined using the reference values:

$$Gr = \frac{\rho_r^2 g(T_h - T_c)H^3}{\mu_r^2 T_r},\ Re = -\frac{\rho_r H^3}{12\mu_r^2}\frac{d\Pi}{dy},\ Pr = \frac{\mu_r c_{pr}}{k_r} = 0.71,\ \epsilon = \frac{T_h - T_c}{2T_r} = 0.3\,.$$

Here we investigate in detail flow arising in the non-Boussinesq mixed convection regime at $(Gr_*, Re_*) = (526921.8, -5179.405)$. The steady y-independent parallel basic flow profiles are shown in Figure 1: downward flow caused by the applied pressure gradient is opposed by the buoyancy forces near the hot wall. The temperature difference between the walls in this regime is 180 K and the fluid transport properties vary significantly across the channel (up to 15%) so that the temperature deviates from a classical Boussinesq linear profile.

Linear stability analysis of such a flow reveals a few interesting features seen from Figure 2. Firstly, the marginal stability curve $Gr(Re)$ has a kink singularity at this set of parameters. Secondly, both critical wave number α

and critical disturbance wave speed c are discontinuous at this point. This situation was previously identified in [1] as a switch between two distinct non-Boussinesq shear driven instabilities, but requires further clarification. Here we investigates in detail flow patterns arising near the "switch" point by means of analysis of a model dynamical system.

Model dynamical system and codimension-2 unfoldings

The real leading disturbance amplification rate curve $\sigma^R(\alpha)$ shown for this regime by the plain solid line in Figure 3 has a peculiar shape: it has two zero maxima at wavenumbers $\alpha_1 = 0.0795$ and $\alpha_2 = 1.1804$. This is the so-called codimension-2 point. Depending on the values of physical parameters in the vicinity of (Gr_*, Re_*) either left or right hump crosses the zero level. The resulting flow pattern depends on nonlinear interaction of two disturbance wave envelopes centered at wavenumbers α_1 and α_2 shown by vertical dotted lines in Figure 3. Both disturbance wave envelopes belong to the same branch of the problem dispersion relation. Hence they have the same physical nature, namely, the shear which is maximal near the inflection point of the basic flow velocity profile. This is consistent with conclusions made in [1], but there it was overlooked that the instability is always caused by the same shear mode (switching the wavenumber) rather than by two distinct modes. The asymptotic behaviour of the system is determined by a relatively narrow neighborhoods of α_1 and α_2 for which the temporal amplification rate σ^R is positive. Since α_1 and α_2 are well separated from each other, in the context of further derivation we consider the corresponding wave envelopes as independent objects subject to weakly nonlinear interaction. Systematic disturbance amplitude expansion about the basic flow solution introduced in [2] and adapted to the codimension-2 analysis in [3] is truncated to third order in amplitudes $A_1(t)$ and $A_2(t)$ corresponding to the disturbances with wavenumbers α_1 and α_2 and reads

$$\begin{aligned}\mathbf{w} = \quad & \mathbf{w}_{000} + |A_1|^2\mathbf{w}^{(1)}_{200} + |A_2|^2\mathbf{w}^{(2)}_{200} + \\ & \Big\{\Big[A_1\left(\mathbf{w}_{110} + |A_1|^2\mathbf{w}^{(1)}_{310} + |A_2|^2\mathbf{w}^{(2)}_{310}\right)E_1 + A_1^2\mathbf{w}_{220}E_1^2 + A_1A_2^*\mathbf{w}_{21-1}E_1E_2^* + \\ & A_2\left(\mathbf{w}_{101} + |A_1|^2\mathbf{w}^{(1)}_{301} + |A_2|^2\mathbf{w}^{(2)}_{301}\right)E_2 + A_2^2\mathbf{w}_{202}E_2^2 + A_1A_2\mathbf{w}_{211}E_1E_2\Big] + \text{c.c.}\Big\}\,,\end{aligned} \tag{5}$$

where $\mathbf{w} = (u, v, T, \Pi)^T$, the first index corresponds to the order of amplitude, the second and the third ones to the powers of $E_1 = \exp(i\alpha_1 y)$ and $E_2 = \exp(i\alpha_2 y)$. The asterisk and c.c. denote complex conjugate. In order for (5) to satisfy equations (1)–(4) the evolution of disturbance amplitudes should be governed by a system of the coupled Landau equations

$$\frac{da_j}{dt} = a_j\left(\sigma_j^R + K_{j1}^R a_1^2 + K_{j2}^R a_2^2\right)\,, \tag{6}$$

$$\frac{d\theta_j}{dt} = \sigma_j^I + K_{j1}^I a_1^2 + K_{j2}^I a_2^2\,, \tag{7}$$

where $A_j = |A_j|\exp(i\theta_j) = a_j\exp(i\theta_j)$, $\sigma_j = \sigma^R + i\sigma^I$ are the eigenvalues of the linearised problem and $K_{jk} = K_{jk}^R + iK_{jk}^I$, $j, k = 1, 2$ are the complex Lan-

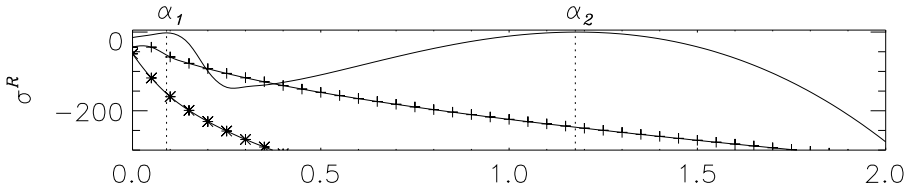

Figure 3: Leading disturbance amplification rates at the codimension-2 point in non-Boussinesq mixed convection.

dau coefficients determined by the orthogonality conditions [2]

$$\langle \mathbf{w} - \mathbf{w}_{000} - A_j \mathbf{w}_{1(2-j)(j-1)}, \mathbf{w}_{1(2-j)(j-1)} \rangle = 0.$$

All coefficients in the above system depend on physical governing parameters thus making analysis of the codimension-2 dynamics a nontrivial task.

First, we consider two equations (6) since they are completely decoupled from the phase equations (7). Using transformations

$$r_1 = a_1 \sqrt{|K_{11}^R|}, \quad r_2 = a_2 \sqrt{|K_{22}^R|}, \quad \mu_1 = -\sigma_1^R, \quad \mu_2 = -\sigma_2^R,$$
$$b = -\frac{K_{12}^R}{|K_{22}^R|}, \quad c = -\frac{K_{21}^R}{|K_{11}^R|}, \quad d = -\frac{K_{22}^R}{|K_{22}^R|}, \quad t \to -t$$

we reduce equations (6) to the canonical form

$$\dot{r}_1 = r_1 \left(\mu_1 + r_1^2 + b r_2^2\right), \quad \dot{r}_2 = r_2 \left(\mu_2 + c r_1^2 + d r_2^2\right) \tag{8}$$

which has been analysed in [4]. Numerical evaluation of the above coefficients at (Gr_*, Re_*) results in $b = 0.925$, $c = -67.340$, $d = 1$, $\mu_1 = \mu_2 = 0$ which corresponds to Type 2a case II of the fixed point with three invariant lines $\left(r_1 = 0,\right.$ $r_2 = 0$, $\left. r_2 = \sqrt{\frac{1-c}{d-b}} r_1\right)$ according to the classification given in [4], Tables 7.5.1 and 7.5.2. In order to unfold this bifurcation note that the four types of equilibria (r_{1e}, r_{2e}) are possible in system (8): a) linearly stable basic flow, (0,0); b) and c) individually bifurcating modes $(\sqrt{-\mu_1}, 0)$ and $\left(0, \sqrt{-\mu_2/d}\right)$; and d) interacting modes $\left(\sqrt{\frac{b\mu_2 - d\mu_1}{d-bc}}, \sqrt{\frac{c\mu_1 - \mu_2}{d-bc}}\right)$. Stability of the above fixed points is determined by the eigenvalues $\lambda_{1,2}$ of a problem obtained by linearizing equations (8) about the equilibrium ($\lambda_{1,2}^R > 0$ for stability because of the time reversion):

$$\lambda_{1,2} = \frac{C_{11} + C_{22}}{2} \pm \frac{1}{2} \sqrt{16bcr_{1e}^2 r_{2e}^2 + (C_{11} - C_{22})^2}, \qquad \begin{array}{l} C_{11} = \mu_1 + 3r_{1e}^2 + br_{2e}^2 \\ C_{22} = \mu_2 + 3dr_{2e}^2 + cr_{1e}^2 \end{array}.$$

Then stability conditions for $d = 1$ are a) $\mu_1, \mu_2 > 0$; b) $\mu_2 > c\mu_1$; c) $\mu_1 > b\mu_2$; and d) is always stable if it exists. Consequently, unfoldings of the codimension-2 point are determined by lines $\mu_1 = 0$, $\mu_2 = 0$, $\mu_2 = c\mu_1$ and $\mu_1 = b\mu_2$. All topologically distinct amplitude flow diagrams near the considered codimension-2 point are presented in Figure 4. Straight lines $a_1 = 0$, $a_2 = 0$ and $a_2 = a_1 \sqrt{\frac{K_{11}^R - K_{21}^R}{K_{22}^R - K_{12}^R}} \approx 1.319 a_1$ in plot (1) are the invariant lines at the codimension-2 point (Gr_*, Re_*). The third of these lines is algebraically attractive so that the distance between it and the trajectories decreases asymptotically as $t^{-3/2}$ while the evolution along the invariant line towards

the origin is $a_1 \sim a_2 \sim t^{-1/2}$. Plots (2)–(7) show all possible unfoldings of a fixed point for case II in [4]. These unfoldings are not discussed in [4] and thus complement the general classification of codimension-2 points given there. The middle plot in Figure 4 relates the unfoldings to the physical parameter space for non-Boussinesq mixed convection.

In order to complete the analysis the phase evolution given by equations (7) has to be considered and in particular the possibility of the phase locking and resonances has to be examined. The phase locking condition is

$$\sigma_1^I - \sigma_2^I + \left(K_{11}^I - K_{21}^I\right) a_1^2 + \left(K_{12}^I - K_{22}^I\right) a_2^2 = 0\,. \tag{9}$$

Differentiating this equation with respect to time and using (6) after some algebra we conclude that (9) may be satisfied only if both amplitudes are constant, i.e. at the stable mixed fixed points $a_{1e}a_{2e} \neq 0$ existing in between the dash-dotted lines in Figure 4 (see plots (4) and (5) for the flow topology). Condition (9) then becomes

$$\frac{\left(K_{11}^I - K_{21}^I\right)\left(\sigma_2^R K_{12}^R - \sigma_1^R K_{22}^R\right) + \left(K_{12}^I - K_{22}^I\right)\left(\sigma_1^R K_{21}^R - \sigma_2^R K_{11}^R\right)}{K_{11}^R K_{22}^R - K_{12}^R K_{21}^R} = \sigma_2^I - \sigma_1^I\,,$$

but it is not satisfied anywhere in Figure 4. Finally, the ratio σ_2^I/σ_1^I remains between 16 and 17 for all points in Figure 4. Hence no strong resonances occur and the performed analysis, accounting for the evolution of amplitude modulus only, is sufficient.

Physical interpretation of results and conclusions

In conclusion we relate the results reported in the previous section to the physical flow under consideration. It has been mentioned in the introduction that the flow is influenced by two competing effects: the buoyancy force and the pressure gradient applied along the channel. The shear driven instability occurs near the inflection point of the basic flow velocity profile (see Figure 1 a). The inflection point is due to the action of the buoyancy forces and appears only if the ratio $Gr/|Re|$ is sufficiently large. For this reason the critical Grashof number increases rapidly with $|Re|$ as seen from Figure 2 (a). At the nearly zero values of $|Re|$ (small pressure gradient) the instability is characterised by almost stationary secondary rolls appearing near the inflection point of the basic velocity profile with the wavelength $\lambda = 2\pi H/\alpha \approx 2.3H$ (Figure 2 b). As the driving pressure gradient increases these rolls start drifting downward with the primary flow and elongate. Thus the pressure gradient has a stretching effect on the flow instability structures. This stretching continues until the size of rolls becomes so large that they start blocking the primary flow too strongly. At the codimension-2 point these very long instability rolls with $\lambda \approx 79H$ break into smaller ones with $\lambda \approx 5.3H$ which drift with larger wave speed (see Figure 2 c) and their "blocking" effect is less profound. Note that such a transition between the flow patterns is not because of the secondary instability of the long rolls, but rather due to a competition between the two distinct flow structures one of which drains the energy from another. This competition is illustrated in Figure 4. For any fixed $Re > Re_*$ the basic flow (plot (2)) first becomes unstable due to the long wave disturbances (plot (3)), which trigger their own distortion at the slightly higher values of Gr (plot (4)). This distortion is supported by draining the energy from the long cells to finer structures (because $K_{21}^R > 0$ and $K_{12} < 0$) through the nonlinear interaction. At even higher values of Gr the shorter rolls become self-supporting by draining the energy

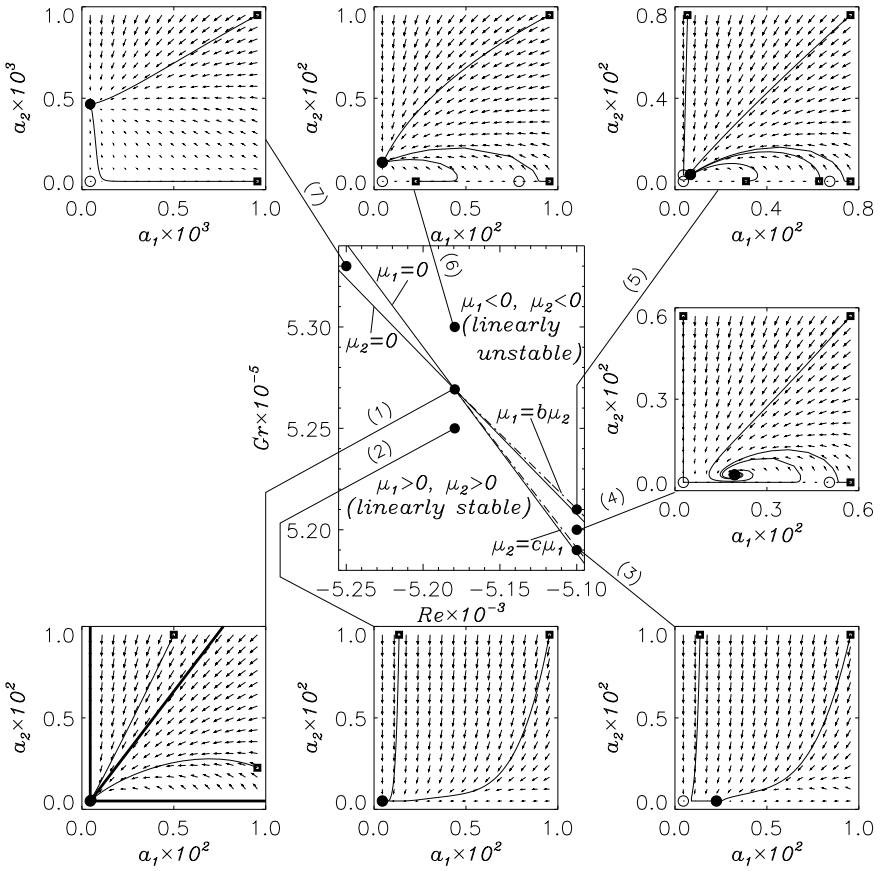

Figure 4: Amplitude flow diagrams and trajectories near the codimension-2 point. Squares and empty and filled circles represent initial conditions and unstable and stable equilibria, respectively.

from the basic flow (σ_2 becomes positive in plot (5)) and eventually destroy the long rolls completely (plot (6)). For $Re < Re_*$ the short wave instability structures always dominate and long rolls cannot be observed (plots (2), (7) and (6)).

Acknowledgement

This work was partly supported by the USQ Early Career Researcher Grant.

References

[1] S.A. Suslov and S. Paolucci, *J. Fluid Mech.*, 1995, **302**, 91–115.

[2] S.A. Suslov and S. Paolucci, *J. Fluid Mech.*, 1997, **344**, 1–41.

[3] S.A. Suslov and S. Paolucci, *Proc. ASME Heat Transfer Division 3*, 1997, HTD-Vol. **353**, 243–250.

[4] J. Guckenheimer and P. Holmes, *Nonlinear Oscillations, Dynamical Systems, and Bifurcations of Vector Fields*, Springer-Verlag, New York, 1985.